PNAS
www.pnas.org

Supplementary Information for

Dissociations between glucose metabolism and blood oxygenation in the human default mode network revealed by simultaneous pet-fmri.

Lars Stiernman Jonasson[12], Filip Grill[23], Andreas Hahn[4], Lucas Rischka[4], Rupert Lanzenberger[4], Vania Panes Lundmark[123], Katrine Riklund[23], Jan Axelsson[23], Anna Rieckmann*[123].

Anna Rieckmann
Email: anna.rieckmann@umu.se

This PDF file includes:

Supplementary Materials and Methods

Maintenance and Manipulation. For the WM maintenance condition, each trial consisted of a target phase where four letters were presented for 2000 ms, a delay period of 3500 ms and a probe letter that was presented for 2500 ms during which participants were required to respond whether the probe corresponded to one of the target letters. Participants responded with their right index finger to indicate “yes” and with the middle finger to indicate “no”. Each trial was followed by a short fixation period of 1000 ms. In the manipulation condition, the timing was identical but the target phase included two letters the probe letter required participants to determine whether the probe corresponded to the subsequent letter in the alphabet of either of the two target letters. This condition requires maintenance and manipulation of the target in WM during the delay period.

Positron Emission Tomography. The reconstructed FDG images were pre-processed in the following steps: (i) motion correction was performed by aligning each volume to the mean volume between minutes 40-45, (ii) spatial smoothing using an 8mm gaussian kernel, (iii) temporal smoothing using a running filter with a [0.5 1 0.5] kernel over three time points. (iv) normalization of *tissue-activity curve* (TAC) in each voxel to the maximum intensity of that voxel.

Magnetic Resonance Imaging

The study specific B0 template was based on 13 participants (data for 10 participants was lost due to an error in the acquisition). The magnitude and fieldmap volumes were normalized to standard space via T1 space and were then averaged to form study-specific templates. These templates were then back-transformed into each of the 23 subjects’ native space for use in FEAT.

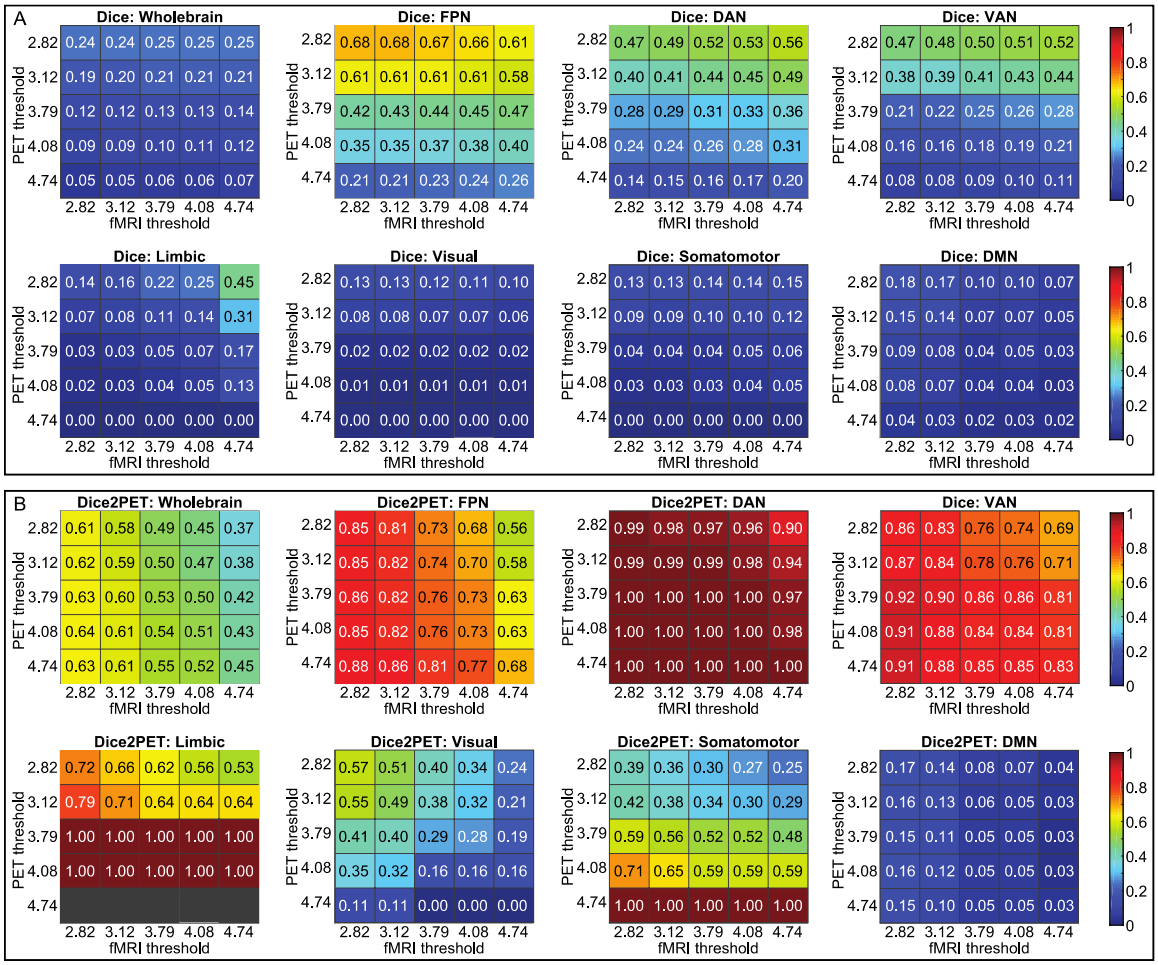

Fig. S1. Dice overlap between BOLD and fPET statistical maps of the manipulation > rest contrast differs depending on functional network. The seven network parcellation from Yeo (1) was used to define functional networks, along with a whole-brain region encompassing all gray matter voxels. Dice overlap was calculated between the BOLD and fPET *t*-maps at different combinations of uncorrected thresholds, corresponding to $p < 0.01$ ($t < 2.818$) to $p < 0.0001$ (4.738) in increments of $p < 0.05$. (A) Original dice overlap scores are shown. (B) As BOLD compared to FDG increases were generally more widespread, an additional overlap score considering the union over the total amount of active PET voxels was calculated for each network. Comparing A and B, the drastically higher overlap scores primarily in DAN, VAN, limbic, visual, and somatomotor networks in B indicates that the voxels with increased FDG overlap with those showing increased BOLD, but that FDG is more focal, and BOLD more widespread. Note, however that this pattern may in part also arise if the modelling statistics for FDG is simply lower than for BOLD, irrespective of physiology (But see Fig S2A-B). Regardless, the multimodal coactivation patterns clearly differ between functional networks, where attention networks show the highest similarity, followed by sensory and motor areas. FPN = frontoparietal network, DAN = dorsal attention network, VAN = ventral attention network, Limbic = limbic network, Visual = visual network, Somatomotor = somatomotor network, DMN = default mode network.

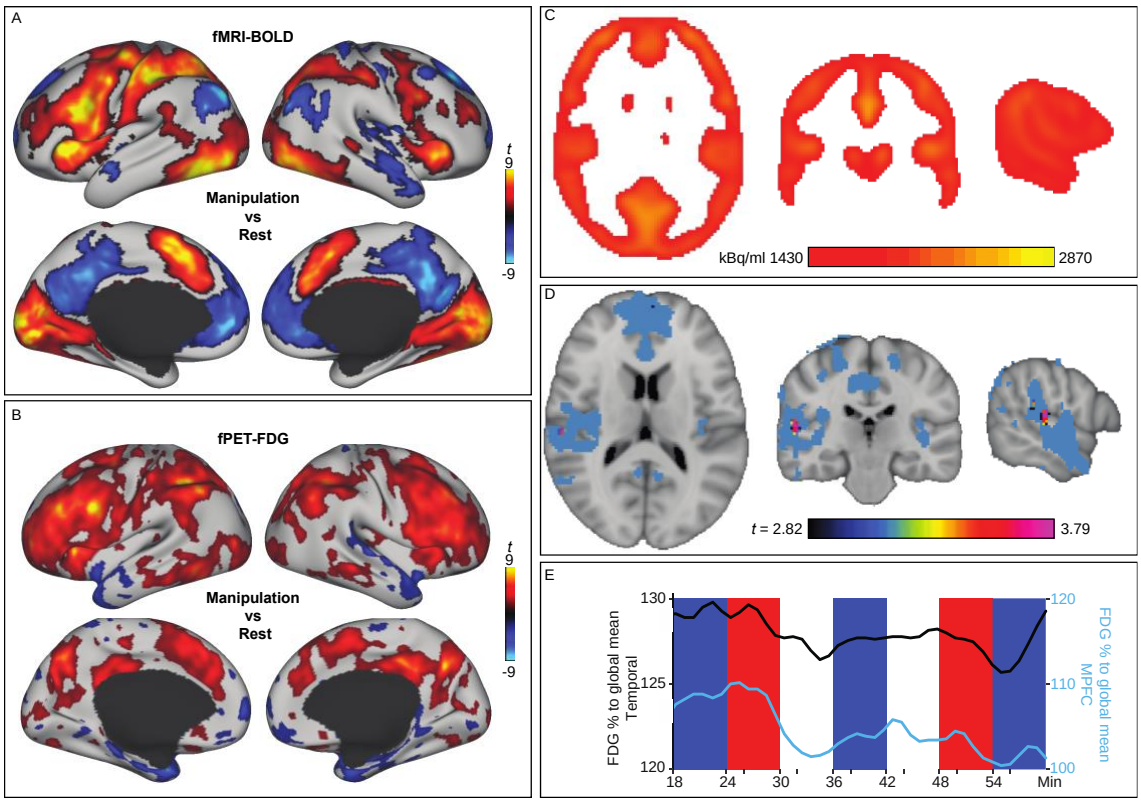

Fig. S2. Decreased glucose metabolism during manipulation compared to rest in areas with NBR was evident in the right temporal lobe and medial frontal pole. (A) Uncorrected fMRI analysis for the manipulation versus rest contrast thresholded liberally at $t > 1.5$. (B) A correspondning uncorrected PET analysis for the manipulation versus rest contrast thresholded at $t > 1.5$. A-B show that the general patterns reported in the main text are not due to sub-threshold signal changes in either modlaity. (C) The whole-brain, corrected (tfce p > 0.05) voxelwise analysis revealed relative decrease in FDG uptake during manipulation compared to rest in bilateral temporal lobe and medial frontal pole only. Because we did not have a-priori hypotheses about the specificity in temporal cortex or regional heterogeneity within MPFC and because these are area prone to spurious result in both fMRI and PET, due to air/fluid-tissue boundaries and proximity to draining veins, we extended our analysis with a control analysis, restricted to voxels with high radioactivity uptake and showing robust BOLD deactivations. The FDG mask used for the analysis retained voxels with its maximum uptake during the full experiment above the 60th percentile, essentially including only cortical grey matter not in the immediate vicinity of large draining veins or fluids. (D) The resulting *t*-test output was masked with significant NBR ($p < 0.05$, *TFCE* corrected). With these additional precautions (which have no effect on the task-related increases reported in the main text), FDG decreases during task (manipulation < rest) were identified only in the temporal lobe, with a peak signal change significant at $p < 0.001$ ($t = 3.79$, uncorrected, two-tailed), and in anterior *medial prefrontal cortex* (MPFC). In order to be able to appreciate the peak and cluster-extent of the clusters, the threshold was lowered to $p < 0.01$ ($t = 2.82$, two-tailed) in this panel. The temporal cluster shown in B appears well within both the gray matter and NBR masks. The fact that decreases converge, at least at a commonly used uncorrected threshold, in temporal cortex shows that a lack of FDG deactivations in core DMN regions such as the posterior DMN is not reflecting a technical limitation to detect decreases. The decrease in MPFC was located at the edge of the mask however, running the risk of being an artefact and should be interpreted with caution. (E) Illustrates dynamic changes in FDG signal within the right temporal cortex peak [MNI coordinates 57 -25 12] and MPFC [-2 62 7] showing increases in rest (blue) and decreases during manipulation (red). Because the kinetic modeling is sensitive to noise in small ROIs the timeseries illustration shows the % difference between FDG signal in the peak and the FDG signal in the rest of the FDG

mask at each time frame, i.e. a model free illustration of dynamic changes in FDG distribution relative to the rest of the brain. A second tick mark was added 2 minutes after the tick mark illustrating the start of a new block to account for the delay in FDG signal change (Fig. S3).

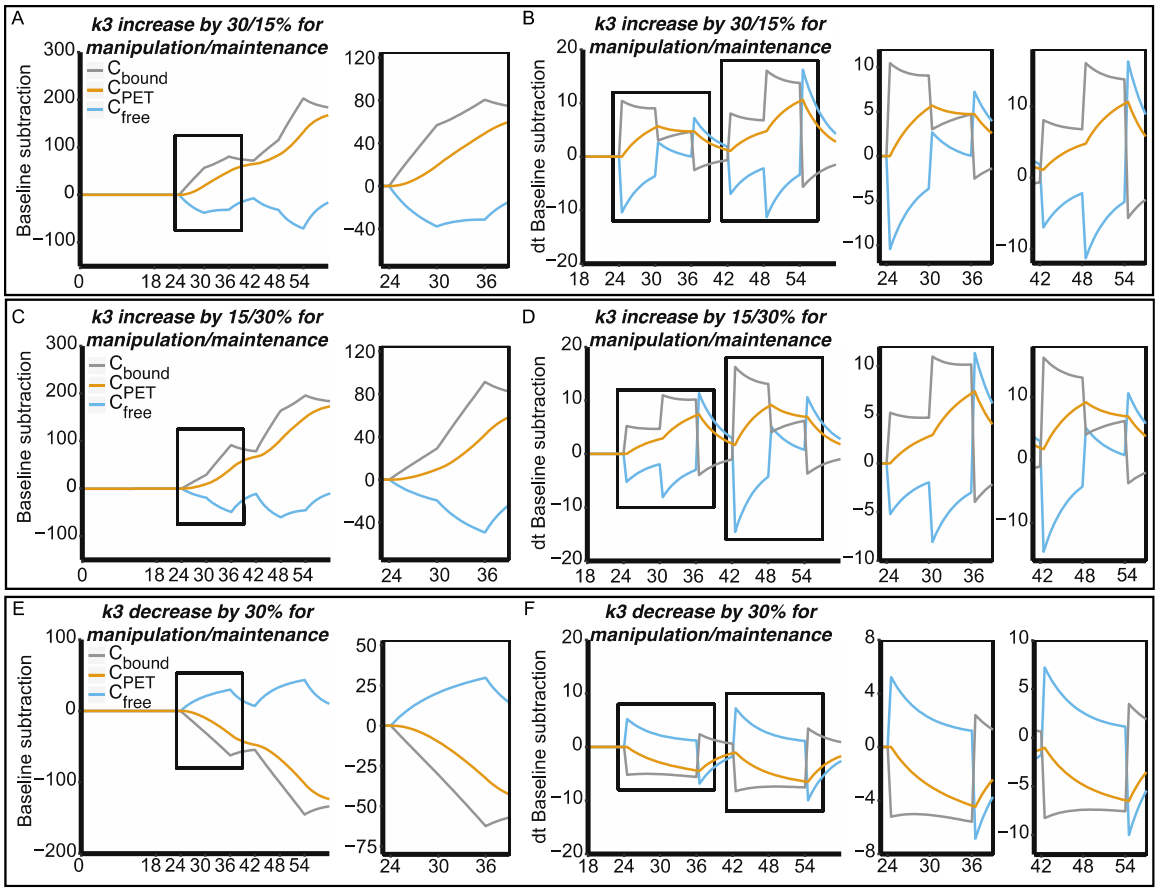

Fig. S3. Supplementary Fig. 3. Simulations of metabolized, free, and tissue concentrations of FDG in response to blocked 6 min increases and decreases in k_3. The arterial input function and values for *K1* (0.1), *k2* (0.15), and *k3* (0.08) from(2) formed the basis for the simulations. k_4 was set to zero, and V_b of 0.04 was used. To simulate the effect on the measured PET signal from differences in metabolic demand between conditions, k_3 was allowed to vary in blocks of 6 min. The concentration of tracer found in the tissue and blood (C_{PET}), corresponding to the signal measured in the PET scanner with real subjects, along with concentrations of free (C_{free}) and metabolized (C_{bound}) tracer was calculated for a 60 min long experiment (24 min of rest, followed by six 6 min blocks in the following order: manipulation, maintenance, rest, maintenance, manipulation, rest). The tissue concentrations under a baseline experiment (no change in k_3 during the 60 min) were subtracted from the concentrations in two activation and one deactivation experiment, resulting in a residual FDG signal reflecting increases or decreases in the rate of glucose metabolism under various conditions. (A) k_3 was set to increase by 30% under the manipulation, and 15% under the maintenance condition. An enlarged view of min 23 to 39 is provided as it illustrates the delay in C_{PET} from a change in k_3 that is due to the interplay between tracer delivery, C_{free}, and C_{bound}. (B) The derivatives from A were plotted along with two enlarged views of both task periods as it clearly shows (i) that the change in slope for C_{PET} in A, being the foundation for fPET, is not immediate (ii) that the slope increases for the full 6 min of a demanding block following a less demanding block, and (iii) that the slope remains positive even for subsequent rest blocks when k3 is equal to the baselines. (C) and (D) the same analyses as in A-B were performed but with maintenance being the more demanding condition. In D it is apparent that the shape of the derivatives in the two panels are close to mirrored as compared to B with only minor differences. The scale is different however, suggesting that (i) the slope estimation in a given block differs slightly depending on the ordering of preceding blocks and (ii) that slope estimations will be higher in later blocks. Consequently, counterbalancing the order of blocks is important in order not to induce a systematic bias when comparing the magnitude of a change between conditions. (E-F) To simulate the response in areas where glucose demand is higher during rest compared to the tasks, k_3 was set to decrease by 30%

during both the demanding and intermediate tasks. As in A-D, the sluggishness of C_{PET} is evident, albeit in the opposite direction. Taken together these simulations show that, irrespective of the direction of k_3 change, the sluggishness of C_{PET} should be taken into account when performing GLM based modelling of changes in the slope of C_{PET}. In theory, this could explain the reduced statistical sensitivity of fPET observed as blocks become shorter(3).

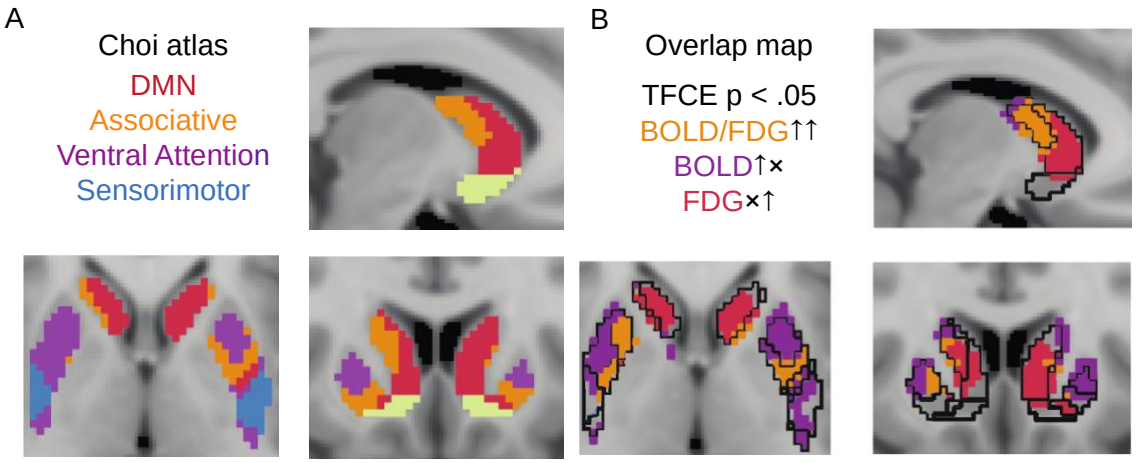

Fig. S4. Differences between changes in BOLD and glucose metabolism in functional divisions of the striatum during working memory manipulation compared to rest. The striatum is a structure with discrete functional areas. Choi and colleagues parcellated the striatum according to their belonging to the seven functional networks, including limbic, associative, attentional, and DMN parcels(4). This seven-network atlas was used for the subsequent comparisons between BOLD signal changes and glucose metabolism in striatum. Similar to the pattern observed in the cortex, PBR and FDG increases overlapped in the dorsal striatum, associated most strongly with FPN. In sensorimotor putamen, PBR were found but no significant FDG increases, likely reflecting the same pattern as generally observed in sensorimotor and motor cortex (i.e. sub-threshold FDG task increases). FDG increases without significant PBR were additionally observed in medial caudate within areas associated most strongly with DMN, akin to the pattern seen in posterior DMN in cortex. However, in contrast to the cortical patterns presented in previous sections, no NBR were observed within the striatal DMN. **a** The Choi atlas (4). **b** The borders of the parcels are outlined along with filled areas where BOLD and FDG increases and their overlap/non-overlap are presented at $p < 0.05$ (corrected). Map of distinct multimodal BOLD and FDG signatures created by assigning colors to voxels based on co-activation or modality specific activations. DMN = *default-mode network*, TFCE = *threshold-free cluster enhancement*.

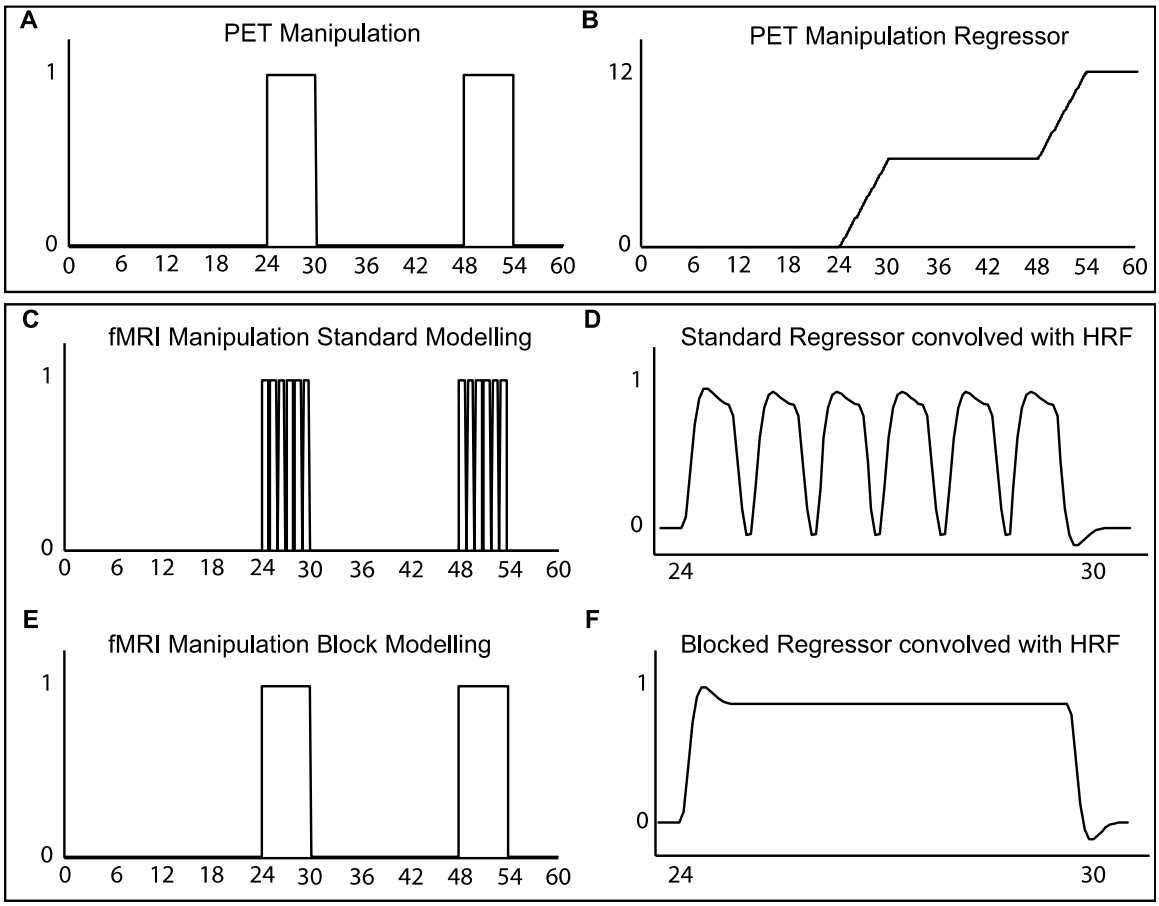

Fig. S5. Modelling of PET and fMRI regressors. (A) The manipulation regressor for PET is shown as a boxcar function, with two 6-minute blocks separated by 18 minutes. (B) To account for the near irreversible binding of FDG, the boxcar function was transformed to a ramp function that served as the final regressor for the GLM analysis, consistent with prior work (2, 5). Further, to account for delay in tracer uptake, the ramp function was shifted two minutes forward in time, i.e. the actual ramping of the manipulation regressor occurred between minutes 26 to 32 and 50 to 56 (Fig. S3). (C) The manipulation regressor for the fMRI data was modelled using standard fMRI modelling, where each short block within the 6-minute task block was modelled as 45s “on” and 15s “off”. (D) A close-up of the standard manipulation regressor between 24 and 30 minutes convolved with a *hemodynamic response function* (HRF). (E) To model the fMRI data similarly to the PET data, an alternative model treated 6-minute task blocks as a continuous “on” period, i.e. excluding the short rest periods between the blocks within blocks. This was done as a control analysis to show in Figure S6 that the difference between the PET and fMRI results reported in the main text were not merely due to a difference in modelling the short rest periods between the one-minute blocks. (F) A close up of the blocked manipulation regressor between 24 and 30 minutes convolved with a HRF.

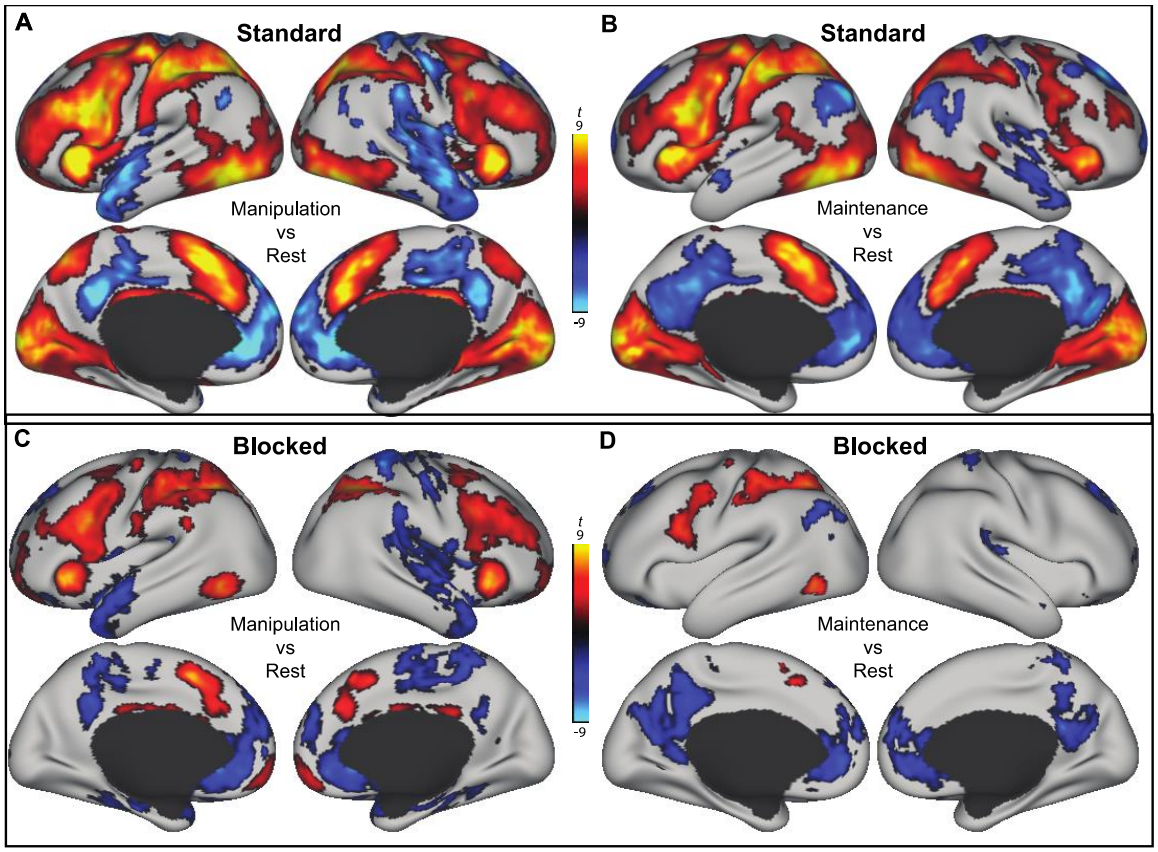

Fig. S6. The overall pattern of task-induced fMRI signal changes are largely similar irrespective of modelling approach. (A) The manipulation versus rest contrast using the standard modelling approach (cf Fig. S5D) reported in the main text. (B) The maintenance versus rest contrast using the standard modelling approach reported in the main text. (C) The manipulation versus rest contrast using the blocked modelling approach (Fig. S5F). (D) The maintenance versus rest contrast is shown using the blocked modelling approach. All images show TFCE corrected results with a threshold of $p < 0.05$. As expected, the standard modelling approach provides higher statistics overall compared to the non-standard blocked approach. A particularly notable difference was observed in visual cortex,where fMRI activation was below threshold, similar to the pattern observed in PET (main text). Hence, the lack of a robust change of FDG in visual cortex may at least in part be attributed to a difference in modelling approach. Importantly however, the NBR observed in DMN remain. Hence, the dissociation between BOLD and FDG observed in posterior DMN is not merely due to modelling one modality as a 6-minute block rather than 6 consecutive blocks within blocks.

Table S1. Peak activation/deactivation foci for the manipulation > rest contrast.

fMRI						PET					
Region	**MNI coordinate**			***t***	***k***	**Region**	**MNI coordinate**			***t***	***k***
Cerebellum	36	-50	-30	14.1	25615	IFG[1]	46	26	20	10.4	4218
Intracalcarine cortex	14	-72	10	6.76		Precentral/MFG[1]	-38	6	30	8.4	3159
Insula[1]	-32	20	-2	12.7	18614	SPL[1]	-28	-54	40	7.3	833
Precentral/MFG	-42	6	30	8.71		ACC[3]	-6	18	32	9.8	783
Paracingulate	-4	14	46	7.75		Precuneus[4]	4	-68	34	8.7	620
Paracingulate	8	28	32	7.93		Lateral Occipital superior[1]	38	-68	48	6.8	612
Putamen	-24	2	6	8.03		PCC[4]	4	-42	34	7.5	552
Thalamus	-10	-22	10	7.5		Insular cortex[3]	-30	24	4	7.9	522
MFG	-32	0	60	12.8		SPL/Angular gyrus[2]	32	-48	42	6.5	352
ACC	-8	24	28	6.58		Caudate[5]	-12	14	2	7.9	345
Caudate	-14	0	18	6.76		Caudate[6]	14	14	8	4.7	262
Supramarginal gyrus	-32	-46	40	8.53		ACC[1]	6	30	28	7.8	173
Lateral occipital superior[2]	30	-66	36	6.02	1360	Temporooccipital cortex[2]	-50	-60	-16	8.3	114
						Lateral Occipital superior[2]	-26	-66	40	5.6	87
MPFC	10	42	-2	-10.8	6568						
STG	62	-24	4	-8.31	5495						
Precuneus/PCC	6	-36	50	-7.93	4560						
Heschl's Gyrus	-42	-20	2	-12.5	2426						
Angular Gyrus	-56	-64	30	-6.64	222						

All coordinates are reported in *Montreal Neurological Institute* (MNI) space. Peak locations were extracted from *t* statistic maps masked using a *threshold-free cluster-extent* (TFCE) correction of $p < 0.05$ and a gray matter probability map of 0.5. To achieve separation of the large fMRI clusters an additional threshold of $t > 5.402$, $p < 0.00001$, was set, and the first ten non-cerebellar clusters are reported below the original cluster. The anatomical naming convention was based on the Harvard-Oxford atlas. *k* = cluster extent, functional networks [1-6] defined by Yeo (1) if cortical and Choi (4) if striatal, [1]FPN, [2]DAN, [3]VAN, [4]DMN, [5]DMN striatum, [6]associative striatum, ACC = anterior cingulate cortex, fMRI = functional magnetic resonance imaging, MFG = middle frontal gyrus, PCC = posterior cingulate cortex, PET = positron emission tomography, SPL = superior parietal lobule, STG = superior temporal gyrus.

SI References

1. B. T. T. Yeo, *et al.*, The organization of the human cerebral cortex estimated by intrinsic functional connectivity. *J. Neurophysiol.* **106**, 1125–65 (2011).
2. M. Villien, *et al.*, Dynamic functional imaging of brain glucose utilization using fPET-FDG. *Neuroimage* **100**, 192–199 (2014).
3. L. Rischka, *et al.*, Reduced task durations in functional PET imaging with [18 F] FDG approaching that of functional MRI. *Neuroimage* **181**, 323–330 (2018).
4. E. Y. Choi, B. T. T. Yeo, R. L. Buckner, The organization of the human striatum estimated by intrinsic functional connectivity. *J. Neurophysiol.* **108**, 2242–63 (2012).
5. A. Hahn, *et al.*, Quantification of task-specific glucose metabolism with constant infusion of 18 F-FDG. *J. Nucl. Med.* **57**, 1933–1940 (2016).